ISSN: 3066-8131
Research Article

Science Set Journal of Physics

Synthesis, X-ray crystallography, spectroscopic characterization, electronic structure investigation and molecular docking studies of single Cobalt (II) metal complex against

Afef Gannouni[1*], Hitler Louis[1], Thierry Roisnel[2], Ernest E. Ekereke[5], Destiny E. Charlie[2] Elizabeth Ukwenya[4], Riadh Kefi[1]

[1]*Laboratoire de Chimie des Matériaux, Faculté des Sciences de Bizerte, 7021 Zarzouna, Tunisie*

[2]*Computational and Bio-Simulation Research Group, University of Calabar, Calabar, Nigeria*

[3]*Department of Pure and Applied Chemistry, Faculty of Physical Sciences, University of Calabar, Calabar, Nigeria*

[4]*Centre de Diffractométrie X, UMR 6226 CNRS, Institut Sciences Chimiques de Rennes, Université de Rennes I, 263 Avenue du Général Leclerc, 35042 Renne, France.*

[5]*Department of Mathematics, Faculty of Physical Sciences, University of Calabar, Calabar, Nigeria*

[*]Corresponding author: Afef Gannouni, Laboratoire de Chimie des Matériaux, Faculté des Sciences de Bizerte, 7021 Zarzouna,Tunisie

Submitted: 02 Jan 2023 **Accepted:** 12 Jan 2023 **Published:** 23 Jan 2023

https://doi.org/10.63620/MKSSJP.2023.1009

Citation: *Gannouni, A., Louis, H., Roisnel, T., Ekereke, E. E., Charlie, D. E., Ukwenya, E., & Kefi, R. (2023). Models for capacitors on a pot plant battery, ppb and impact on lifetime of 3v-batteries with traditional electricity, Sci Set J of Physics 1(1), 01-16.*

Abstract

The present work undertakes the study of novel hybrid compound, which have been obtained due to the interaction of organic and inorganic entities with cobalt transition metal. The novel solid-state complex (2-ethylpiperaziniumtetrachlorocobaltate (II)), abbreviated as 2EPCO, was synthesized and characterized using several physic-chemical techniques, such as single crystal X-Ray diffraction analysis, spectroscopic measurements, intra and intermolecular studies and DFT calculation, thermal and biological properties. It crystallizes in orthorhombic system with space group Pbca. The atomic arrangement of $(C_6H_{16}N_2)$ $[CoCl_4]$ can be described as an alternation of organic and inorganic layers along the b and c axis, which are interconnected by hydrogen bonds. Hirshfeld surface, topological-In-moleculs (AIM) and natural bond orbital (NBO) were conducted to investigate intermolecular interactions. The reduced density gradient (RDG) was used to study non-covalent interactions. In this study present the crystal structure studies, characterization, electronic properties investigation, and the in-silico biological activities of (C6H16N2) [CoCl4] hybrid material against 6PXZ, 6RK2 and 6Y8Q bacterial receptor proteins. The electronic structural properties were elucidated within the framework of density functional theory (DFT) computations at the PBE0-D3/gen/6-311++G (d, p)/LanL2DZ level of theory and the associated results were compared with experimental data to investigate the antioxidant properties of single Cobalt (II) metal complex. The interaction between the ligand and the receptor proteins has the following binding affinities: 5 kcal.mol^{-1}, -6 kcal.mol^{-1} and -5 kcal.mol^{-1} for 2EPCO_6PXZ, 2EPCO_6RK2 and 2EPCO_6Y8Q protein-complex interactions, respectively. However, the commercial drug when bind with the selected protein had lower docking scores: cycloserine_6PXZ, cycloserine_6RK2 and cycloserine_6Y8Q with respective binding affinity values of -4.0 kcal.mol^{-1}, -4 kcal.mol^{-1} and -1 kcal.mol^{-1}. Finally, thermal analysis techniques (ATD/TG) were carried out to account for the thermal decomposition of complex.

Graphical Abstract

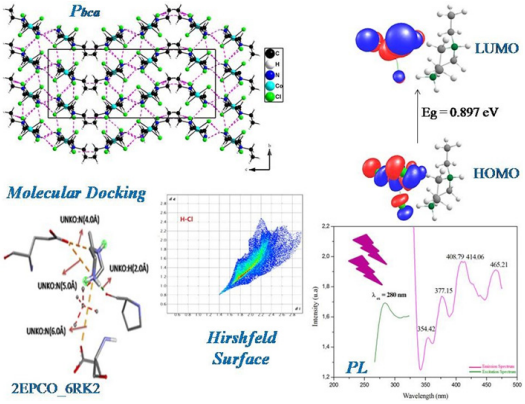

Keywords: Hybrid Compound; Crystal Structure; Spectroscopy; DFT Calculation Electronic Properties; Molecular docking

Introduction

Coordination compounds based on transition metal have attracted a great of attention because they bring together the properties of organic and inorganic molecule. Over the years, it is observed there is a wide interest in the development of natural and synthetic antioxidants

as they have been proven to function in the prevention of various diseases [1]. Antioxidants serve as a means to neutralize free radicals; reactive oxygen species (ROS) and in turn protects cells and reduce oxidative damage. These free radicals are unstable atoms that can damage cell membrane, DNA, proteins and lipids. They are formed when there is a cleavage of chemical bonds in a molecule. Reactive species are as a consequence of cellular processes. They are categorized into reactive oxygen species (ROS) and reactive nitrogen species (RNS). Reactive oxygen species include; superoxide radical anion, hydrogen, hydroxyl radical, peroxides; such as peroxides of protein and lipids. ROS plays an essential function in biological systems, diseases, by causing injury in organisms, resulting in cases like arthritis, cancer, heart and liver diseases, atherosclerosis and emphysema. Alternatively, ROS can act as mediators of damage in cell structures, which includes lipids and membranes, proteins and nucleic acids. Recent developments have proven that the most effectively medium to eliminate ROS is through the use of antioxidants. ROS bring about oxidative stress, when there an imbalance in the production of these species, also distorts its capacity to repair cellular damage. Many literatures have shown interest on metal-based toxicity. Many investigations have focused on metal-based toxicity. Very limited studies have been carried on Cobalt (II) complexes, yet there have been a whole lot of interesting studies done to investigate the antioxidant activity of metal complexes. Azam, M, et al, performed a DFT studies to investigate the antioxidant activity of Schiff base metal complexes of 2- aminopyridine [2]. Through the application of FRAP method, it was revealed that Nickel (II) complex was the most active. Tsiepe et al carried out a DFT study in Vacuo and in solution, to reveal the antioxidant properties of Kanakugiol through hydrogen atom transfer, electron transfer and M2+ + M2+ = Cu (II) or Co (II) Ion coordination ability mechanisms [3]. This study was conducted using B3LYP/M06-2x/B3P86/6-31+G (d, p)/6-311+G (d, p) level of theory. This study revealed that Cu (II) complex is the most stable complex, on the basis of its greater binding strength. Swiderski et al carried out a theoretical study on the antioxidant potential of the 3d transition metals [Co(ii), Ni(ii), Cu(ii), Zn(ii)] complexes respectively with Cichoric acid Alzahrani et al synthesized Mn (II) complexes, carried out DFT investigation on the antioxidant activity via enhancing superoxide dismutase enzymes, confirmed by in- silico and in-vitro ways [4-5]. Oueslati et al DFT studies, molecular docking, single crystal investigation, Hirshfeld surface analysis, physico-chemical characterization, and in vitro investigation of the antioxidant activity of a novel hybrid complex using TD-DFT/B3LYP/6- 31+G (d, p) level of theory [6]. The results obtained in this work noted that hybrid materials can be considered as a promising biological active substance that can be helpful in the field ofbiological medicine as an antioxidant. Therefore, this work is aimed at investigating the synthesis, X-ray crystallography, electronic structure investigation using the density functional theory, and molecular docking studies to investigate the antibacterial potential of single Cobalt (II) metal complex.

Experimental

Synthesis of ($C_6H_{16}N_2$) [CoC_{l4}]

The monocrystals of (C6H16N2) [CoCl4] were obtained by dissolving in a concentrated hydrochloric acid solution (37%) and a stoichiometric mixture of (2-ethyl) piperazines and a solution of hexahydrated cobalt chloride (CoCl2.6H2O) in a minimum volume of water. Stirring for 30 min, until the formation of a clear mixture without any precipitate. After one week, evaporation leads to the formation of stable crystals of 85% yield. The percentages of elemental atoms are: C: 22.72%; N: 8.8%; Co: 18.59%; Cl: 44.74% and H: 5.05%. This synthesis follows the following pattern:

$$C_6H_{14}N_2 + CoCl_2.6H_2O + 2HCl \xrightarrow{H_2O} (C_6H_{16}N_2\,[CoC_{l4}]$$

X-ray single crystal structural analysis

A suitable crystal for X-ray diffraction single crystal of a new centrosymmetric compound (C6H16N2)[CoCl4](0.370 x 0.250 x 0.050 mm3) was selected and mounted with a cryoloop on the goniometer head of a D8 Venture diffractometer equipped with a (CMOS) PHOTON 100 detector, using monochromator radiation (λ (Mo-Kα) = 0.71073 Å) at 150(2) K. Crystal structure has been described in orthorhombic symmetry and Pbca (I.T # 61) centric space group. The structure was solved by dual-space algorithm using the SHELXT program, and then refined with full-matrix least-squares methods based on F2 (SHELXL program [7-8]. All non-Hydrogen atoms were refined with anisotropic atomic displacement parameters. Except Hydrogen atom linked to N6 Nitrogen atom that was introduced in the structural model through Fourier difference maps analysis, H atoms were

finally included in their calculated positions and treated as riding on their parent atom with constrained thermal parameters. A final refinement on F2 with 2999 unique intensities and 128 parameters converged at ωR(F2) = 0.0703 (RF= 0.0357) for 2408 observed reflections with (I >2σ). Drawings were made with Diamond [9].

Spectroscopic Measurements

The infrared spectrum was measured at room temperature in the 400–4000 cm-1 frequency range with a Nicolet IR200 FT-IR spectrometer. The IR spectroscopy is used to identify the functional groups and to determine the molecular structure. The UV-Vis absorption was measured at ambient temperature with a Perkin Elmer Lambda 35 UV/Vis spectrophotometer in the range of 200 – 800 nm. The photoluminescence analyses were performed at room temperature by Perkin Elmer LS55 Spectrofluorimeter.

Density functional theory (DFT) details

The Kohn-Sham density functional theory (DFT) computation was carried out for the geometry optimization of the studied surface at PBE0/Gen methods by assigning 6-311++G (d,p) and LanL2DZ basis set [10]. The log files generated from the Gaussian 16 software were analyzed employing the GuassView 6.0.16 software package for the frontier molecular orbital (FMO) analysis, graphical representation of the highest molecular orbital and the lowest unoccupied molecular orbital was done by Chemcraft program v 1.6. QTAIM analysis was done with the Multiwfn 3.7 software program [11-12,13]. The natural bond orbitals (NBO) computations for the studied surface in order to determine the second order perturbation energy and charge transfer, was done using the NBO 7.0 module available in Gaussian 16. The Hirshfeld surface analysis and finger plots for the studied surface was carried out using crystal explorer 3.1, the PyMOL and Biovia v 21 was employed for the molecular docking carried in this study [14-15,16]. Finally, the highest occupied molecular orbital (HOMO) and the lowest unoccupied molecular orbital (LUMO) and the energy gap for the studied compound, was obtained using equation 1: Egap(eV) = ELUMO (eV) – EHOMO (eV) (1)

Molecular docking protocol

Using three different bacterial infection proteins (6PXZ, 6RK2 and 6Y8Q) retrieved from the protein data bank (pdb). We have conducted molecular docking using Biovia discovery Studio, autodock vina and PyMOL respectively [16-15]. The proteins were prepared using biovia discovery studio. The synthesized structure of 2EPCO was optimized and converted into a pdb format for docking analysis. This study used molecular docking to perform virtual screening on the synthesized of present structure in order to better understand its biological functions and potential as a bacterial infection disease therapy candidate. The following proteins (6PXZ, 6RK2 and 6Y8Q) were prepared by removing the water molecules; editing and defining the active sites for proper ligand interactions, deleting the native ligand and adding the polar hydrogen. The grid box was created using a 1 Å spacing for the target protein after the active site residues of the target proteins were chosen. The AutoDock Tool's ligand

menu was used to import the ligand molecules in PDB format. All non-rotatable bonds were then made rotatable, and the ligand and complexes were then saved in pdbqt format. The ligands, protein target, and configuration file containing the dimensions of the grid box—that is, the center x, y, and z values—were used to perform docking using AutoDock Vina. Also, PyMOL program was used for visualization of the 3D of the ligand protein interaction [17]. (6PXZ) protein was selected based on prior studies; the majority of the retinol in the bloodstream of mice infected with Salmonella is bound by SAA proteins (6PXZ). Hepatocytes and other cells manufacture SAA proteins during an acute infection, which are then released into the bloodstream. The majority of SAA is known to interact with high- density lipoprotein in the blood of infected mice (HDL). However, we discovered that the majority of the circulating retinol was linked to the little portion of SAA proteins that are free to circulate and are the main retinol-binding form in vivo. On the other hand, the used of (6RK2) protein was based on its ability to regulate the timing to inhibit bacterial virulence expression and control human immune response. SghA breaks SA from SAG. Because SA is a crucial signaling molecule in the defense against several pathogenic infections, these findings show a 2-way chemical signaling cross-talk that was previously unknown to occur during the co evolution of microbes and hosts and provide mechanistic information about host-bacteria interaction. Literature review shows that Toxin-antitoxin (6Y8Q) systems are essential for bacterial adaptability, including defense against antibiotic attack and bacteriophage infection hence the choice for the selected proteins for this study.

Thermal analysis

The simultaneous TG-DTA analysis curves of the title compound were carried out in argon atmosphere at a heating rate of 5°C.min-1 in the temperature range 25–700 °C on a sample of 11 mg.

Results and discussion

Structure description

The compound (C6H16N2)[CoCl4] crystallizes in the orthorhombic system with the Pbca space group with a = 11.4324 (10) Å, b = 9.6121(7) Å, c = 23.720 (2) Å and Z = 8 to T = 150K.

Table 1 shows the recording conditions and refinement results. Fig. 1 is a representation of the asymmetric unit of the 2EPCO structure. This unit contains a tetrahedral anion [CoCl4]2- and an organic cation $[C_6H_{16}N_2]2+$. Fig. 2 shows that the atomic arrangement of the compound 2-ethylpiperaziniumtetrachloridocobaltate (II) can be described by infinite chains along the c axis. The chains are connected to each other via hydrogen bonds of type N–H…Cl and C–H…Cl to build the three-dimensional structure. Each cobalt atom is surrounded by four chlorine atoms with Co-Cl distances ranging from 2.2493 (8) to 2.2823(8) Å. In addition, the Cl-Co-Cl angles vary from 105.54(3) to 117.28(3)°. These values are similar to those found in the bibliography [18-19].

The Baur method is used to describe the mean distortion indices (DI) and angles calculated in $[CoCl_4]$ of 0.0075 for Co1-Cl and 0.0306 for Cl-Co1-Cl [20]. The asymmetrical complex unit contains a single independent crystallographically independent diprotonate organic cation. The C-N distances are between 1.484(4) and 1.513(3) Å and the C-C distances ranges from 1.511(4) to 1.523(4) Å. Besides, the N-C-C angles vary between 109.9(2) and 112.4(2)°. The C-N-C angles are between 111.0(2)

and 112.2(2)°.

Table 1: Crystallographic data and structure refinement parameters of $(C_6H_{16}N_2)[CoCl_4]$.

Crystal data	
Chemical formula	$(C_6H_{16}N_2)$ $[CoCl_4]$
Crystal color	Blue
Formula weight (g/mol)	316.94
Crystal system	orthorhombic
Space group	Pbca
a, b, c (Å)	11.4324 (10), 9.6121 (7), c= 23.720 (2)
α = β = γ (°)	90
Volume V (Å3)	2606.5 (4)
Z	8
Crystal size (mm3)	0.370 x 0.250 x 0.050
Radiation (Wavelength (Å))	0.71073
F (000)	1288
Density (calculated), (mg/m3)	1.615
Diffractometer	D8 venture diffractometer
Theta range for data collection (°)	2.474 – 27.507
Reflections collected	13689
Index ranges	h = -12/14; k= -12/12; l = -30/30
No. of measured, independent &	2999
observed [I > 2s(I)] reflections	2408
Absorption coefficient/[mm-1]	2.479
Abs.correction	Multi-Scan
Max and min. transmission	0.900 and 0,717
Goodness-of-fit on F2	1.077
Final R indices [I > 2s(I)]	R1 = 0.0357, wR2 = 0.0703
R indices [all data]	R1 = 0.0528, wR2 = 0.0789
Largest diff. peak and hole [e. Å3]	-0449, 0.424

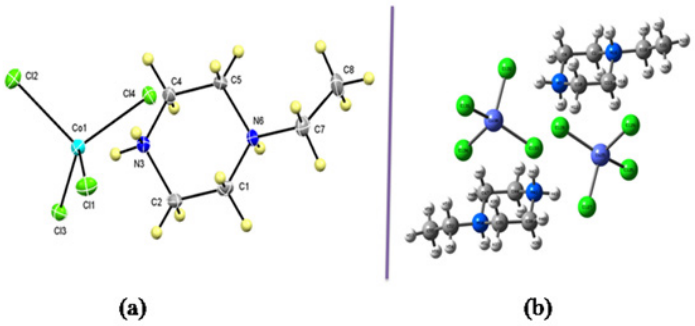

Figure 1: (a) Asymmetric unit and atom labeling scheme of (C6H16N2)[CoCl4] and (b) optimized geometry of the cluster model used in the DFT and TDDFT calculations.

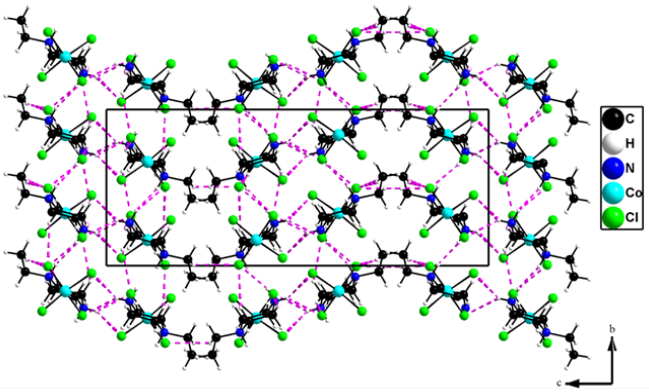

Figure 2: Projection along the c-axis of (C6H16N2)[CoCl4]. The dotted lines indicate hydrogen bonds.

The crystalline structure is stable by establishing the hydrogen bonds formed between the organic and inorganic groups. The distances and angles describing these hydrogen bonds are presented in Table 2. In this structure, the two azotes (N3 and N6) and carbons (C4 and C5) act as acceptors of hydrogen bonds whereas the chlorine atom Cl1 is not involved in hydrogen bonds. The H…Cl distances range from 2.3 to 2.80Å. The N–H…Cl and C–H…Cl angles range from 122 to 159°. These values are similar to those found in the bibliography [21].

Table 2: Summary of selected bond distances (Å) and bond angles (°) for the comparative studies of Co25 compound calculated at DFT/PBE0-D3/Gen/6-311++G (d,p)/LanL2DZ.

D – H ⋯ A	D – H (Å)	H ⋯ A (Å)	D ⋯ A (Å)	D – H ⋯ A (°)
N3 - H3A ... Cl4	0.98 (3)	2.35 (3)	3.2188 (3)	159 (3)
N 3 -H3B ... Cl2_#1	0.85 (3)	2.53 (3)	3.240 (3)	141 (3)
N3 - H3B ... Cl3_#1	0.85 (3)	2.76 (3)	3.293 (2)	122 3)
C4 – H4A ... Cl2_#2	0.99	2.80	3.692 (3)	149.7
C4 - H4B ... Cl2_#3	0.99	2.80	3.573 (3)	135.1
C5 – H5A ... Cl4_#2	0.99	2.74	3.679 (3)	158.1
N6 - H6 ... Cl2_#3	0.88 (3)	2.38 (3)	3.214 (2)	158 (3)

Electronic structure investigation

The optimized geometry of the studied compound was carried out using the Gauss View program, using DFT/PBE0/GEN/6-311++G (d,p)/LanL2DZ method. Selected optimized bond lengths and bond angles are presented in Table 3. In the table 3, the selected bond distances for the X-ray diffraction data, are compared with that obtained from the density functional theory data. It can be deduced that the deviation in bond distances between the experimental and theoretical data were obviously small, this is as a result of the intermolecular interactions. The maximum deviation in bond distance for Co1-Cl2 and Co1-N3 are 0.126 and 0.106 Å, respectively. The molecular visualization of the crystal structure is represented in Fig. S 1.

Table 3: Hydrogen bonding parameters (Å, °) for $(C_6H_{16}N_2)[CoCl_4]$.

Experimental	Density Functional Theory (DFT)	
Bonds	***Bond distance (Å)***	***Bond distance (Å)***
$Co_1 – Cl_1$	2.249	2.357
$Co_1 – Cl_2$	2.303	2.429
$Co_1 – Cl_3$	2.268	2.290
$Co_1 – Cl_4$	2.282	2.184
$Co_1 – N_3$	4.005	3.899
	Bond angles (°)	***Bond angles (°)***
Cl_1-Co_{25}-Cl_2	105.55	100.44
Cl_3-Co_{25}-Cl_4	107.24	116.31
N_3-Co_{25}-N_4	37.87	37.98

Electronic structure investigation

The optimized geometry of the studied compound was carried out using the Gauss View program, using DFT/PBE0/GEN/6-311++G (d,p)/LanL2DZ method. Selected optimized bond lengths and bond angles are presented in Table 3. In the table 3, the selected bond distances for the X-ray diffraction data, are compared with that obtained from the density functional theory data. It can be deduced that the deviation in bond distances between the experimental and theoretical data were obviously small, this is as a result of the intermolecular interactions. The maximum deviation in bond distance for Co1-Cl2 and Co1-N3 are 0.126 and 0.106 Å, respectively. The molecular visualization of the crystal structure is represented in Fig. S 1.

From the Fig. S 1, the studied complex 2EPCO has a cobalt centroid that is covalently bonded to four chlorine atoms. The cobalt to chlorine bond distances range from 2.249 to 4.005 Å in the experimental and a range of 2.184 to 2.429 Å for the density functional theory (DFT) calculation. The bond distances from cobalt to the axial position substituent for the complex with bond Co1 – Cl1 is 2.249 Å for the experimental and 2.357 Å for the theoretical. Notably, the bond distances observed in the density functional theory are slightly higher than that of the experimental except for the bond Co1-Cl4 bond distance 2.194 Å.

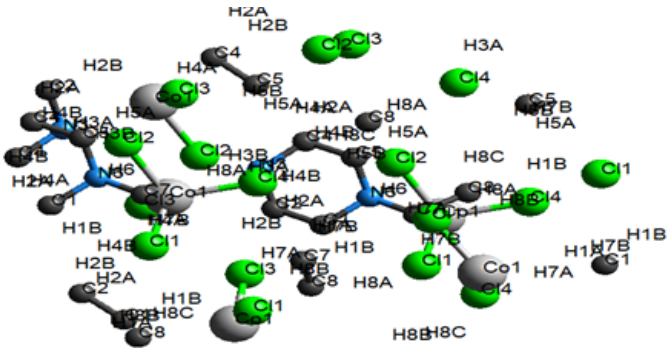

Figure S - 1 : Molecular visualization of the crystal structure $(C_6H_{16}N_2)[CoCl_4]$ with omitted hydrogen bond and numbers for purpose clarity

Hirshfeld Surface

The Hirshfeld surface of the studied compound is obtained us-

ing the Crystal Explorer 3.1 program. The molecular Hirshfeld surface generated for this compound is obtained using a standard surface resolution with 3-D d_{norm} surfaces which is mapped over a fixed color scale of -0.4204 (red) to 1.3056 Å (blue) and a shape index that is mapped in the range of -1.0000 and 1.000 Å as displayed in Fig.3. In the d_{norm} surface, the thick dark red colors indicate the H…Cl interactions, while the other visible parts in the d_{norm} surface generated, corresponds to the H...H contacts [22]. From the Hirshfeld surface generated, the white color represents the intermolecular distance close to the Van der Waals contact. In addition, the 2-D finger plot for the surface has been generated and is depicted in Fig.4. The finger plot examines the main intermolecular contacts and its distribution in percent. It is observed from the finger plot, the contribution of the contact H-Cl to the total surface is 98.3% with the remaining 1.7% making up the remaining percentage of the total surface. Fig. S2 displays the visualization of the intermolecular interaction of the studied surface. It is observed that the strong intermolecular interactions in the title compound are between the H – Cl bonds.

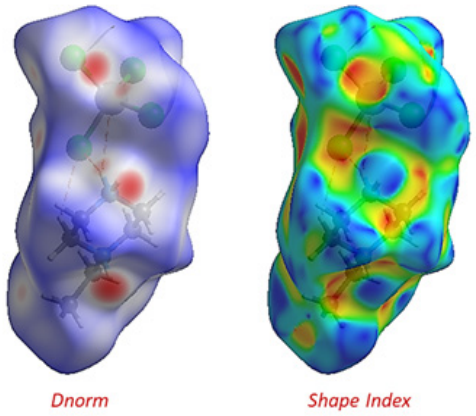

Figure 3: d_{norm} surfaces for $C_6H_{16}Cl_4CoN_2$ mapped over a fixed scale of -0.4204 (red) to 1.3056 Å (blue) and shape index of $(C_6H_{16}N_2)[CoCl_4]$ molecule.

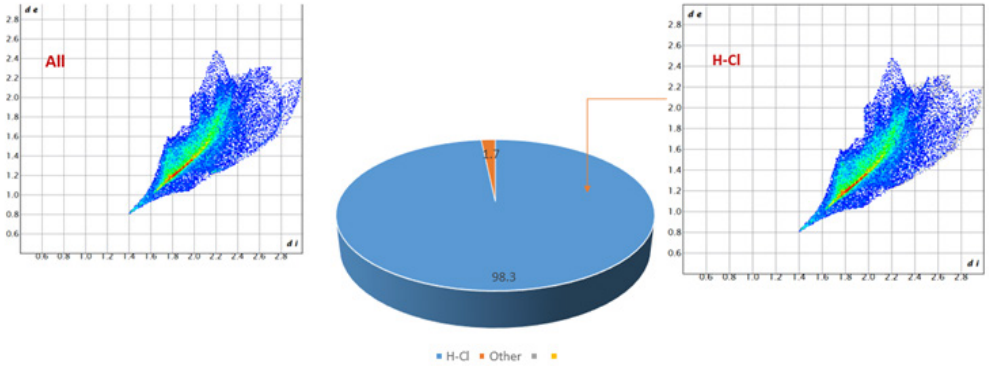

Figure 4 : 2-D Finger plots of 2EPCO compound

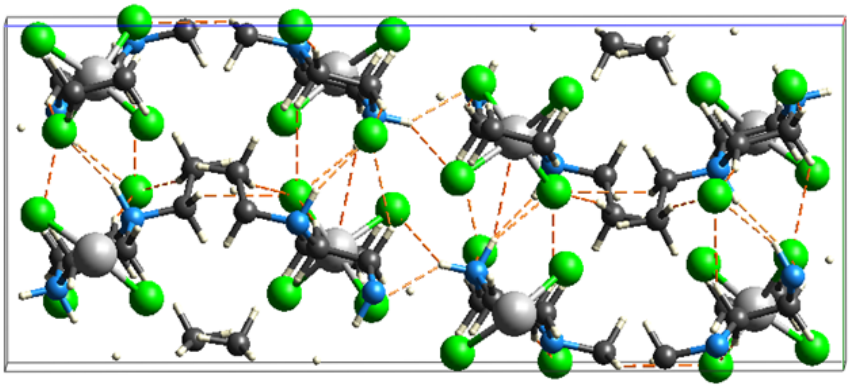

Figure S 2 : Intermolecular Interaction of $(C_6H_{16}N_2)[CoCl_4]$ (Co_2)

Vibrational Study

To obtain more information on the vibrational behaviour of the functional group of the developed compound and to confirm the results of X-ray diffraction, a vibrational study of infrared absorption was carried out. The experimental (1) and theoretical (2) IR vibration spectra of (C6H16N2)[CoCl4] are shown in Fig. 5. Attempts to assign experimental and theoretical absorption bands are reported in Table S – 1. Infrared absorption spectra show vibration bands between 3300-2720 cm-1 and 3410-2727 cm-1 corresponds to symmetric and asymmetric valence vibrations of NH, NH2, CH2 and CH3 groups of experimental and theoretical results, respectively. While, the symmetric and asymmetric deformation vibrations of NH2 and CH2 groups are between 1660-1490 cm^{-1}, these vibrations are confirmed by the DFT calculation by the presence of these bands in the same range; 1661 and 1459 cm-1. The deformation vibration band detected at 1510 cm-1 corresponds to the HCCN off-plane vibrations. Indeed, the symmetrical and asymmetrical deformation vibrations of the HCC group located between 1440 and 1450 cm^{-1}. The vibration range between 1380 and 820 cm-1 attributed to the transition deformation vibrations of the clusters {HCCN, HCCN

and HCCH}. The bands between 475-580 cm^{-1} and 761-284 cm-1 correspond to the symmetrical and asymmetrical deformation vibrations of experimental and theoretical CCN groups, respectively. In the end, the bands between 380-223 cm^{-1} formed by the vibration of the Co-Cl anionic group, these vibrations are similar to non-aromatic compounds [26-28]. The correlation between the experiment and the calculation shows a correlation factor equal to 0.99521 (Fig. S 3). There is a good correlation between these two spectra and the small observed difference justified by the fact that the experimental spectrum is measured in the crystalline (solid) phase, while that simulated is calculated for single molecules (gaseous).

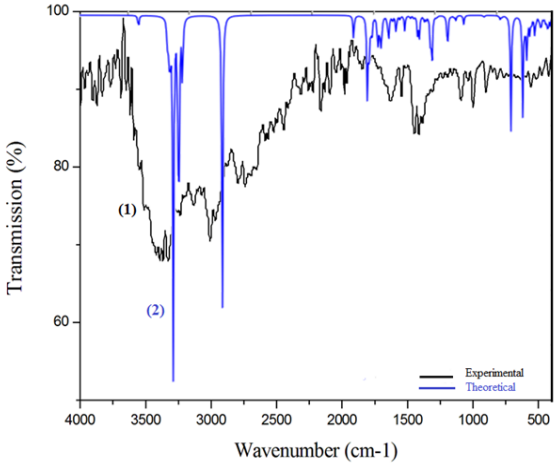

Figure 5: Experimental and theoretical FT-IR Spectra of $(C_6H_{16}N_2)[CoCl_4]$

Table S – 1: Assignments of IR vibrational modes in $(C_6H_{16}N_2)[CoCl_4]$

Frequency (cm^{-1})		Attribution
IR Experimental	IR Theoretical	
3300 - 2987	3410, 3126	ν_s (-NH)
2830	3177, 3175, 3167, 3157	ν_s (CH2)
	3091, 3075, 3052, 3151, 3082	
	3049, 3162, 3121, 3090, 3083	
2800	3167, 3135	ν_{as} (CH2)
2760 - 2720	3121, 2727, 2740	ν_s (-NH2)
2723	3135	ν_s (CH3)
1660	1661	δ_s (NH2)
1650	1658	δ_{as} (NH2)
1545	1546, 1545, 1544, 1527, 1509	δ_s (CH2)
	1522, 1548, 1531, 1534, 1535	
	1512, 1459	
1510	1531, 1512, 1458, 1381, 1341	τ_{as}(HCCN)
1490	1509, 1459	δ_{as} (CH2)
1450	1467, 1446, 1442, 1312, 982	δ_s (HCC)
	1441, 1341, 1281, 1198, 1083, 1372,	
	1447, 1313, 1343, 1279, 1196, 985	
1440	1447, 1467	δ_{as} (HCC)
1380	1381, 1279, 1020, 825, 248, 1168	τ_s(HCCN)
	1123, 236, 1196, 985, 1343	
	1167, 1123, 1019	
1350	1347, 1196	τ_s (HCHCl)
1120	1137, 1046, 909, 1068, 1032	ν_s (CC)
	1123, 1083, 860, 840, 826, 372	
1095	1137, 1123, 1046, 909, 894, 825	ν_s (CN)
820	839	τ_s (HCCH)
580	761, 598, 477, 452, 597	δ_s (CCN)
475	476, 284	δ_{as} (CCN)
--	380, 377, 249, 247, 223	ν_s (CoCl)
--	281	ν_{as} (CoCl)

--	249	τ_s (NCCN)
--	223, 163	ν_s (ClH)
--	173, 159, 147, 109, 103, 97, 95, 60	δ_s (ClCoCl)
--	140, 113, 112, 109	γ_s(ClClClCu)
--	132, 60, 9	τ_s (ClCoClH)
--	113	δ_s (ClHN)
--	74	δ_s (CoClH)
--	36	τ_s (NHClCo)
--	32	τ_s (ClHNC)

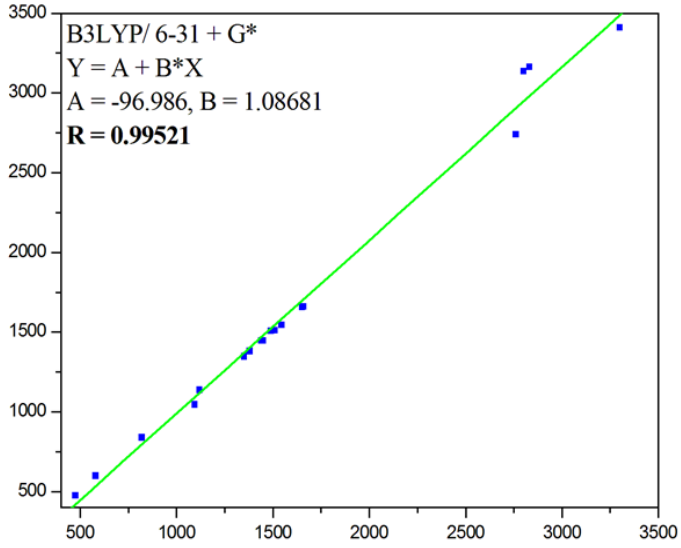

Figure S 3: Correlation graph between the experimental and calculated wavenumbers (cm^{-1}) of 2EPCO

Optical Study

The UV-Visible spectra of title compound are illustrated in Fig. S 4. This crystalline structure presents an intense and wide absorption in the wavelength range 550-750 nm. This band corresponds to three absorption limits respectively at 620 nm, 650 nm and 680 nm (spectrum in orange). These bands correspond to the transfer of load between the cationic and anionic part. The quantum calculation confirms these experimental results by the presence of an intense absorption band of maximum around 763.256 nm (spectrum in blue). The Kubelka- Munk theory is given by the following form: F(R) = (1-R)/2R, where R is the reflectance of this compound and F(R) is the function of Kubelka-Munk [29]. The Fig. S 5(a) and Fig. S5 (b) show the percent reflectance spectra and the F(R) curve (K.M). Using the TAUC method to determine the gap energy of 2EPCO compound, the spectrum F(R) h□)2 as a function of h□ shows that this value is equal to 1.3 eV (Fig. 6). Our synthesized compound has a lower gap energy than that found for a cobalt-based similar compound {(C5H8N3)2 [CoCl4].H2O} (Direct method; Eg = 1.67 eV) [30]. The detailed assignments of transitions of the title compound are presented in Table 4. Fig. S6 represented the optical transmission spectrum of (C6H16N2) [CoCl4]. The crystal transmits light in the wavelength domains {300-610 nm and 710-1000 nm}. In addition, the wavelengths of transparency are equal to 300 nm and 610 nm, respectively. The absorption of our studied compound is in both domains (UV and visible) indicates that our crystal could be used for optical applications as a current separator.

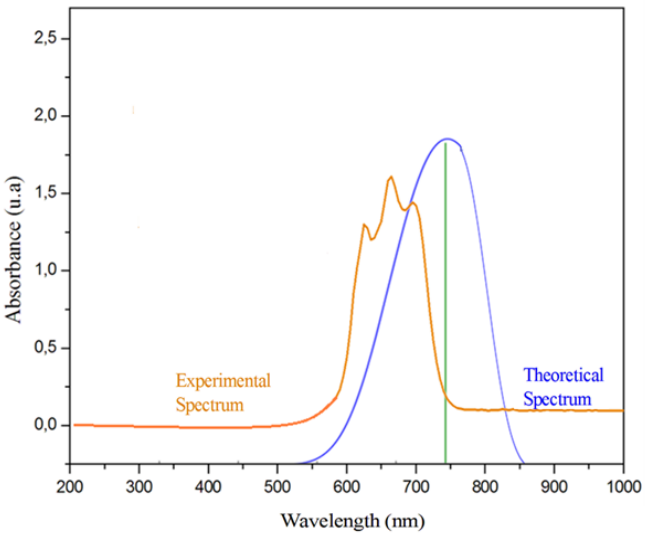

Figure S 4: Correlation graph between the experimental and calculated wavelength (nm) of $(C_6H_{16}N_2)[CoCl_4]$

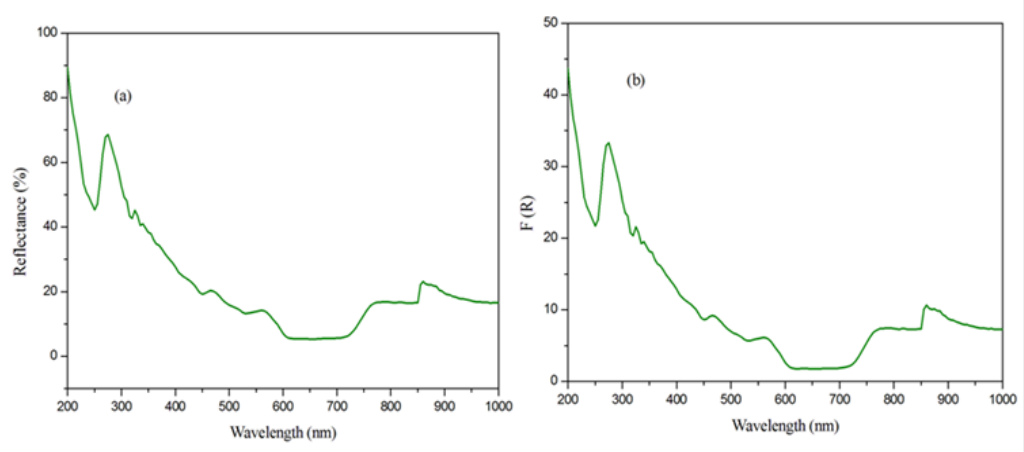

Figure S5: (a): The diffuse reflectance spectra and **(b):** the Kubelka-Munk absorption spectra of $(C_6H_{16}N_2)[CoCl_4]$

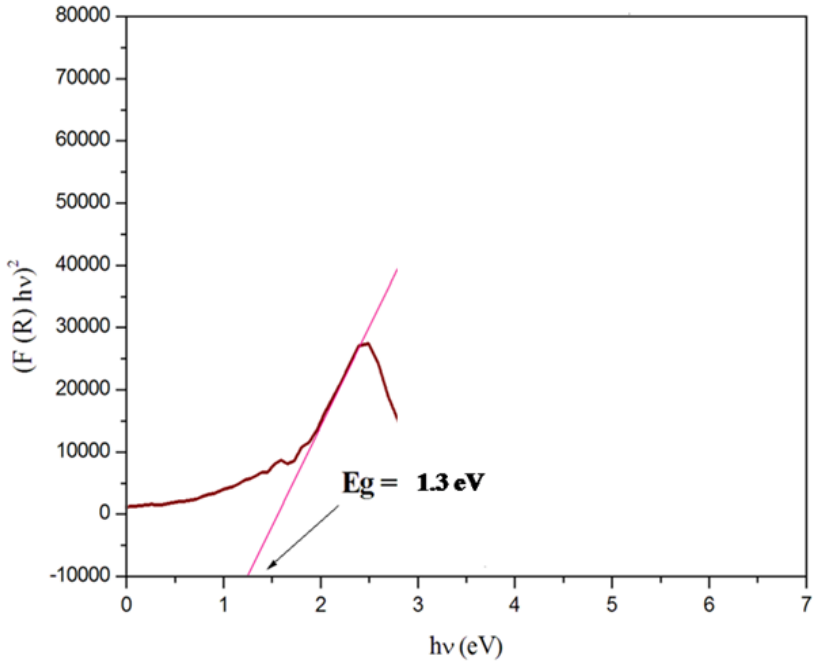

Figure 6: Energy dependence of (F(R) hν)2 versus photon (hν) for $(C_6H_{16}N_2)[CoCl_4]$

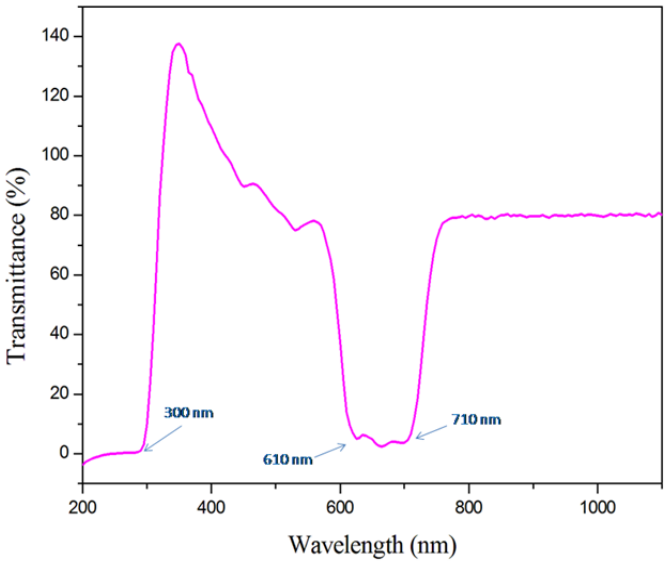

Figure S6: Optical transmittance spectrum of 2EPCO

Table 4: Main calculated optical transitions for the cluster with oscillator strength and major contribution. A comparison between the theoretical and experimental absorption features of $(C_6H_{16}N_2)[CoCl_4]$

Experimental	Theoretical			
Wavelength (nm)	**Wavelength (nm)**	**Transition (nm)**	**Oscillator strength**	**Nature (%)**
620	--	TC		
650	--	TC		
680	763,256	TC	0,0041	H→ L (98 %)

In order to understand the nature of the stability and reactivity of the Co complex, the highest occupied molecular orbital (HOMO), the lowest unoccupied molecular orbital (LUMO) and the energy gap (Egap), were computed for the complex 2EPCO [31]. The stability of the complex is as a result in the energy gap value obtained as a result of the difference in HOMO-LUMO value. According to the FMO theory, the HOMO acts as electron donor, while the LUMO acts as an electron acceptor. The quantum chemical descriptor derived also from the HOMO-LUMO value includes; chemical potential (μ), chemical hardness (η), electrophilicity index (ω) and global softness (σ). Using Koopman's theorem, equation (2)-(5) was employed to calculate the following electronic descriptors, and the results obtained is presented in Table 5

$$\sigma = 1 / 2\eta = 1 / E_{HOMO} - E_{LUMO}$$

$$\mu = E_{HOMO} + E_{LUMO} / 2$$

$$\eta = E_{HOMO} - E_{LUMO} / 2$$

and $\omega = \mu^2 / 2\eta$

Table 5: FMO table for the studied compound calculated at DFT/PBE0/Gen 6-311++G(d,p)/LanL2DZ.

Complex	Co25
HOMO (eV)	-4.374
LUMO (eV)	-3.477
Energy gap	0.897
IP	4.374
EA	3.477
E	1.115
H	0.449
Minus μ	-3.926
EFL	3.926

The HOMO and LUMO value of the studied complex is giving as -4.374 eV and -3.477 eV respectively, giving rise to an energy gap with value 0.897 eV, which depicts that the Co compound has a stable structure [32].To understand the stability of the chemical species and to resists electrocharge transfer within the environment, the chemical hardness plays an important role. A low value obtain for the chemical hardness indicates lower stability and high reactivity of the studied compound. The chemical hardness, global softness, chemical potential and electrophilicity index of the studied compound can be evaluated using the HOMO-LUMO energy values of the Co compound [33].The ionization potential value shows that the energy value is 4.374 eV is needed to remove electron from the HOMO, and the lower value of the electron affinity (EA = 3.477 eV) indicating that the Co(II) readily accepts electron to form bonds. The visualization of the highest occupied molecular orbital (HOMO) and the

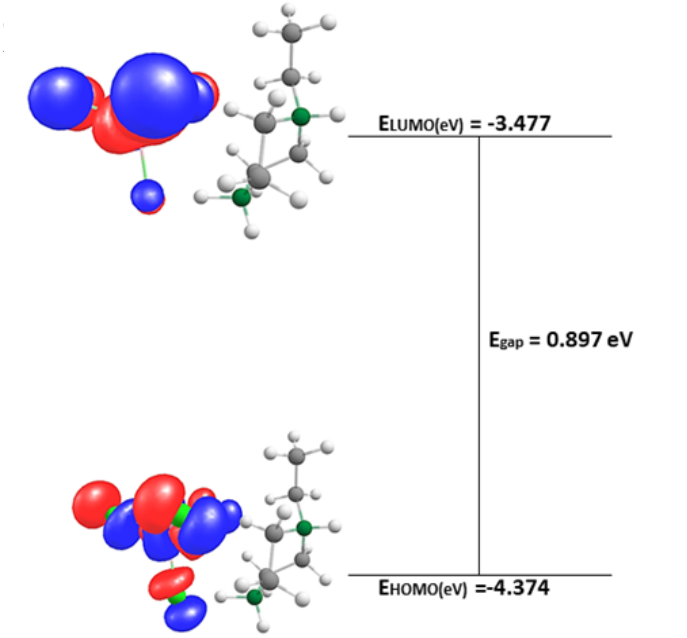

Figure 7: Optimized Iso-surface HOMO - LUMO plot of 2EPCO compound

Photoluminescence properties

The photoluminescence spectrum of the compound $(C_6H_{16}N_2)[CoCl_4]$ was recorded at room temperature, using an excitation wavelength of λex = 280 nm (see Fig. 8). This spectrum has four distinct absorption: a photoluminescence intensity including the maximum wavelength emission observed at λem= 410 nm attributed to a charge transfer from the excited state to the fundamental state of metal cations. While, the bands around 354 nm and 377 nm clearly indicate the contributions and presence of the phenomenon of charge transfer between central cobalt and chlorine atoms. In addition, the intense band around 465 nm probably comes from a transfer of charge between the anionic groups with the organic cation.

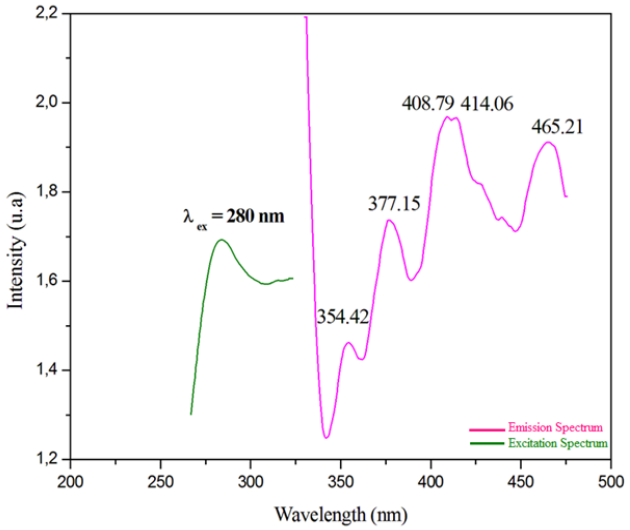

Figure 8: The emission spectra of $(C_6H_{16}N_2)[CoCl_4]$

Absorption of the excitation spectrum at λem = 410 nm confirms the correct wavelength choice at 280nm. Finally, the compound studied shows a violet luminescence at an excitation at 280 nm.

Natural Bond Orbital (NBO)analysis

Natural bond orbital analysis was carried out for this study in order to gain more understanding of the stabilization energy (E2) of the studied compound through charge transfer [34]. In this study, the charge transfer shall be between the donor (i) and acceptor (j) orbitals. The NBO analysis is also an excellent measure used in investigating the intra- molecular and intermolecular bonding and the interaction arising from chemical bonds in the compound. NBO analysis provides necessary knowledge of the charge transfer pattern of the studied system, and also provides the order of stability in the compound [35].The charge transfers were carried out with DFT/UPBEPBE/Gen/Auto level theory. Values of the second order perturbation energy change in diagonal elements and the Fock matrix is presented in Table 6.

Table 6: The second order perturbation energy (E^2) for the studied complexes calculated at DFT/PBE0-GD3/6-311++G(d, p)/LanL2DZ basis level.

Complex	Donor(i)	Acceptor(j)	E^2 kcal/mol	E(j, i)	F(I, j)
$C_6H_{16}C_{l4}CoN_2$	σ^*Co_{25}-Cl_{29}	σ^*Co_{25}-Cl_{26}	126.79	0.02	0.184
	$Lp^*(5)Co_{25}$	σ^*Co_{25}-Cl_{29}	35.21	0.04	0.097
	$Lp(3)Cl_{26}$	$Lp^*(5)Co_{25}$	25.08	0.53	0.151
	$Lp(3)Cl_{27}$	$\sigma^{\wedge*}C_1$-C_2	20.26	0.63	0.155
	$Lp(3)Cl_{29}$	$Lp^*(5)Co_{25}$	19.32	0.94	0.180
	$Lp^*(5)Co_{25}$	$\sigma^{\wedge*}Co_{25}$-Cl_{26}	15.02	0.06	0.080
	σ Co25-Cl_{27}	$\sigma^{\wedge*}C_2$-H_7	10.35	0.82	0.117
	$Lp(1)Cl_{27}$	σ^*Co_{25}-Cl_{27}	8.26	0.93	0.112
	σ^*Co_{25}-Cl_{29}	σ^*Co_{25}-Cl_{28}	5.99	0.13	0.107

The highest energies for this study were carefully selected. Equation (6) was employed for the calculation of the stabilization energy for the studied compound [36].

$$E^2 = \Delta E = -q\, F^2\, i,j/^i\, E - E$$

From equation (6), E2 is the perturbation energy, q represents the donor occupancy, $\Delta E_{i,j}$ is the change in the diagonal elements and F(i,j) is the Fock matrix. The highest perturbation energies selected for this study as presented in Table 5, reveals that the values of the energies with respect to the donor and acceptor decreases greatly from

126.79 kcal.mol-1 to 35.21 kcal.mol-1and thereafter, decreases slightly from 35.21 kcal.mol-1to 25.08 kcal.mol^{-1}> 20.26 kcal.mol^{-1} > 19.32 kcal.mol^{-1} > 15.02 kcal.mol^{-1} > 10.35 kcal.mol^{-1} > 8.26 kcal.mol^{-1} > 5.99 kcal.mol^{-1}. Hence, the compound $(C_6H_{16}N_2)[CoCl_4]$exhibits greater stability due to its large perturbation energy value despite the weak interactions between the adsorbents and the absorber.

Table 7: Docking energy values (ΔG in Kcal.mol-1) of synthesized compound 2EPCO With 3 proteins (6PXZ, 6RK2 and 6Y8Q), and conventional Drug with same proteins.

MODES	6PXZ_ 2EPCO	6RK2_ 2EPCO	6Y8Q_ 2EPCO	6PXZ_ CYC-LO	6RK2_ CYC-LO	6Y8Q_ CYC-LO
1	-5.1	-5.7	-5.3	-3.7	-4.6	-1.3
2	-5.1	-5.6	-5.3	-3.6	-4.4	-1.2
3	-5.1	-5.6	-4.8	-3.6	-4.4	-1.1
4	-5.0	-5.6	-4.7	-3.6	-4.3	-1.1
5	-4.9	-5.6	-4.6	-3.5	-4.2	-1.0
6	-4.8	-5.6	-4.6	-3.4	-4.0	-1.0

7	-4.8	-5.5	-4.5	-3.4	-3.9	-1.0
8	-4.8	-5.5	-4.5	-3.4	-3.9	-1.0
9	-4.7	-5.5	-4.4	-3.3	-3.8	-1.0
Average Binding Affinity	-5.0	-6.0	-5.0	-4.0	-4.0	1.0

Molecular electrostatic potential surface (MEPS)

The molecular electrostatic potential (MEP) of the compound under investigation was calculated using the calculation method B3LYP/LanL2DZ, using the Gaussian 09 software. The dispersion of molecular electrostatic potential in the $(C_6H_{16}N_2)[CoCl_4]$ structure is between -0.115 a. u and 0.115 a. u. The sites of negative electrostatic potential are on the chlorine atoms of the anion $[CoCl4]^{2-}$; on the other hand, the sites of positive electrostatic potential located on the hydrogen of the nitrogen atoms in the cation $[C_6H_{16}N_2]^{2+}$ (Fig. S 7).

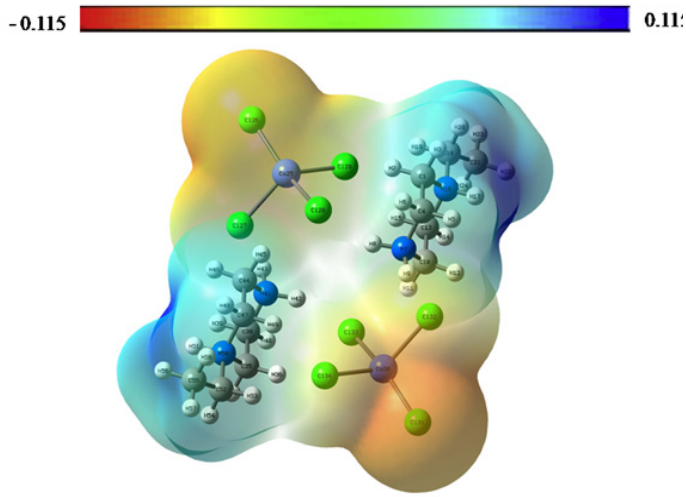

Figure S7: Molecular electrostatic potential surface (between -4.191 and 0.290) Of title compound

Reduced Density Gradient (RDG) analysis

The weak interactions play an important role in many of chemical, physical or biological phenomena [37]. They can be used in various applications such as hydrogen storage for renewable energies [38]. Reduced density gradient (RDG) is a very popular and powerful method for analyzing weak interactions such as Van der Waals interactions, repulsive interactions, and hydrogen bonds using a simple color code. The RDG approach is based on the charge density introduced [39-40]. Fig. S 8(a) gives a visualization of non covalent interaction in the molecular space of $(C_6H_{16}N_2)[CoCl_4]$molecule by using VMD and Multiwfn programs , respectively [41-42]. Fig. S 8(b) illustrates the RDG function versus the electron density ρmultiplied by the sign of the second eigen value of λ2 2EPCO. Through a color code we can differentiate between different regions of interactions, this figure highlights regions of color that allows us to describe the type of interaction. When sign (λ2)ρ take a negative value, we have strong attractive interactions (blue color). The last case, we have Van der Waals interactions when sign (λ2)ρ is close to zero (green color). Strong repulsive interactions when

sign (λ2)ρ have a positive value (red color). Moreover, the blue spot between the chloride atom carried by the nitrogen atom and the chloride atom indicates the formation of a strong attractive interaction N–H...Cl. In addition, the green plates with slight brown located between the organic and inorganic entities, are attributed to Van der Waals interactions and the elliptic red plate located in inorganic part [CoCl4]2- is related to repulsive interactions.

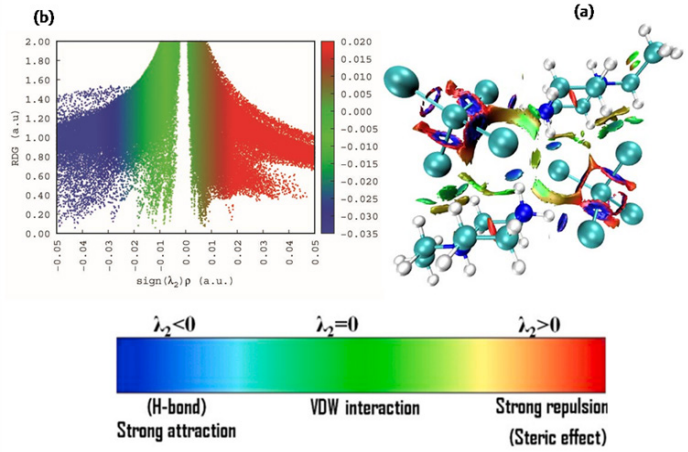

Figure S8: Representation of different types of interactions in the monomer (a). Graph of the reduced density gradient vs. sign (λ2) ρ of $(C_6H_{16}N_2)[CuCl_4]$ (b).

Quantum theory of atoms in molecules (QAIM) analysis

Richard F. W Bader et al, method for quantum theory of atoms in molecule was employed for the topological study carried out in this work [43]. The QTAIM analysis is aimed at giving additional insights about the studied molecule. It provides information surrounding the property of molecules at the bond critical point (BCP) [44]. The topological parameters which includes; the density of all electron ρ(r), Lagrangian kinetic energy G(r), Laplacian of electron density ∇2ρ(r), Hamiltonian kinetic energy K(r), energy density H(r), and the potential energy V(r) [45]. These parameters enable one to determine the interactions and bonds formed between cobalt and chlorine. The values of the Laplacian of electron density ∇2ρ(r) and the energy density H(r) values, enables for the classification of bond as strongly covalent, partially covalent and non-covalent respectively. For values of ∇2(r)<0 and H(r)<0 it indicates the presence of a strong covalent bond, while for values of ∇2(r)>0 and H(r)<0 it indicates the presence of a partial covalent bond and for values of ∇2(r)>0 and H(r)>0, it indicates the presence of a non-covalent bond. The values of the bond critical point and the topological parameters are presented in Table S2. As observed in Table 4, the values of the Laplacian of electron density has positive values from the studied compound i.e∇2(r)>0, indicating the accumulation of the electron density in the region of two bounded atoms, this agrees with [46]. The bonds and values of ∇2(r) and H(r) are giving as; $Co_{25} - Cl_{26}$ (0.165, -0.165), $Co_{25} - Cl_{27}$ (0.145, -0.124), $Co_{25} - Cl_{28}$ (0.165, -0.165) and $Co_{25} - Cl_{29}$ (0.255, -0.238) respectively.

Table S 2: QTAIM table for the studied compounds calculated at DFT/PBE0/Gen/6-311++G(d,p)/LanL2DZ method

Complex	Bonds	BCP	ρ(r)	∇² (r)	G(r)	K(r)	V(r)	H(r)	ELF	Ɛ
	$Co_{25}Cl_{26}$	46	0.737	0.165	0.578	0.165	0.743	0.165	0.293	0.091
	$Co_{25}Cl_{27}$	65	0.569	0.145	0.488	0.124	0.612	0.124	0.197	0.008
2EPCO	$Co_{25}Cl_{28}$	46	0.737	0.165	0.578	0.165	0.743	0.165	0.293	0.091
	$Co_{25}Cl_{29}$	51	0.921	0.255	0.876	0.238	0.111	0.238	0.276	0.157

The result shows that the bond between cobalt and chlorine is a partially covalent bond. This result confirms that there exists a greater binding strength between cobalt and chlorine in the studied complex.

Mulliken Population Analysis and Natural Population Analysis
The natural population analysis of the charges present in the studied complex has been calculated using the Mulliken population analysis, this calculation was done by employing the DFT/PBE0/Gen/6-311++G(d,p) [47]. The atomic charge was investigated because it affects the dipole moment, electronic structure, polarizability and many other molecular properties of the studied system [48]. Mulliken atomic charge describes how the distribution of charges is carried out in the various sub shells in the molecular orbital. The charges

obtained in this study are presented in Table S 3. Notable observation of the values presented in Table S 3 indicates that the sum of Mulliken charges is in the range of -0.0000 at the low side to 1.0000 at the high side at the Hatree-Fock level. As observed in Table S 3, the atoms C1, C4, H5, H6, H8, H9, H10, H11, H12, H13, H17, C18, C19, H21, H22, H23, H24 and

Cl27 all have positive atomic charge values respectively while C2, C3. H7, H14, N15, N16, C19, H20, Co25, Cl26, Cl28 and Cl29 respectively, have negative atomic charge values. Also, it can be observed that all the hydrogen atoms of the natural population analysis have 0 a.u. The values of the carbon atoms for the Mulliken population analysis are lesser than that of the natural population analysis (Fig. S 9).

Table S3: Mulliken Atomic Charge and Natural Population Analysis at PBE0/6-311++G(d,p) basis set of title compound

Atoms	Mulliken Charges	NPA
C1	0.050743	-0.25761
C2	-0.04451	-0.33882
C3	-0.41323	1.99913
C4	0.092784	1.99914
H5	0.234869	0
H6	0.182533	0
H7	-0.87328	0
H8	0.143124	0
H9	0.164585	0
H10	0.147013	0
H11	0.174972	0
H12	0.104991	0
H13	0.134661	0
H14	-0.05328	0
N15	-0.14223	1.99944
N16	-0.14223	1.99942
H17	0.126889	0
C18	0.25636	1.99913
C19	-0.43106	1.99927
H20	-0.065	0
H21	0.142811	0
H22	0.145007	0
H23	0.130322	0
H24	0.074114	0
Co25	-0.64009	17.99771
Cl26	-0.22094	9.99963
Cl27	0.506821	9.99914
Cl28	-0.03297	9.99959
Cl29	-0.2179	9.99962

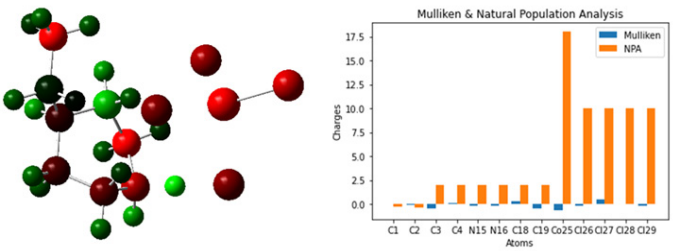

Figure S9: Atoms represented by Colors of calculated atomic charge values from the Mulliken population analysis of 2EPCO

Thermal analysis

Fig. S 10 shows the ATD-TG curves obtained during the decomposition of the compound $(C_6H_{16}N_2)[CoCl_4]$. The endothermic peak at 280 °C is due to the removal of two molecules of HCl. A series of exothermic peaks of 2EPCO compound in the most intense is located at 550°C contributes to the combustion of the organic entity. At the end of the experiment we observed a black deposit mixed with the $CoCl_2$ residue.

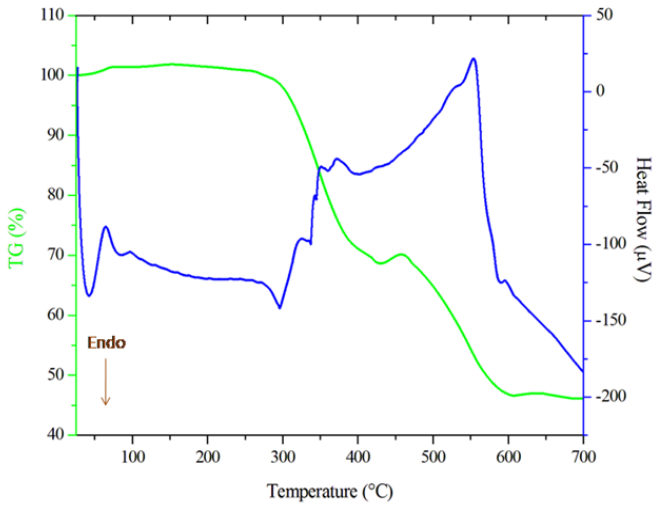

Figure S10: Simultaneous curves of thermogravemetric analysis and differential thermal analysis of 2EPCO

Molecular Docking Analysis

Molecular docking has recently been employed by computational drug design in predicting the binding affinity and compatibility of ligand and proteins interactions. Herein we employed molecular docking approach to determine the compatibility of the studied ligand and the respective bacterial receptor proteins (6PXZ, 6RK2 and 6Y8Q). Evaluation of the synthesized ligand's affinity for binding with 6PXZ, 6RK2 and 6Y8Q was done. The obtained result was further compared with a commercial drug cycloserine with access code (DB00260). The binding poses for the synthesized ligand molecule into the three different receptors were determined as well as the binding poses for the commercial drug with the three proteins. Different poses are produced based on the overall score (dock score). The overall score serves as a measure of the binding affinity of a ligand-receptor complex as presented in table 7. From Fig. S 11, it was observed that the interaction between the ligand and the receptor proteins has the following binding affinities: -5 kcal.mol-1, -6 kcal.mol-1 and -5 kcal.mol-1 in 2EPCO_6PXZ, 2EPCO_6RK2 and 2EPCO_6Y8Q, respectively. However, the commercial drug when bind with the selected protein had lower docking scoresi. ecycloserine_6PXZ, cycloserine_6RK2 and cycloserine_6Y8Q with respective binding affinity values of -4 kcal.mol-1, -4 kcal. mol-1 and -1 kcal.mol-1. The synthesized ligand exhibits the best ligand pose binding energy values, indicating that it is strongly compatible with the receptors. Whereas, the commercial ligand was observed to have lower binding scores, these results shows that our new scoring function for the prediction of binding affinity is useful for molecular recognition and virtual screening for bacterial infection drug design. Furthermore, the selected ligand structure with the highest hydrogen bond from the 9 poses where represented in 3D Structure as shown in fig. 9. From the presentation above, the protein- ligand complexes is stabilized in the binding pocket of receptor 2EPCO_6PXZ by one hydrogen bond with the Amino-acid; UNKO:H(2.9Å), only steric interactions were observed in 2EPCO_6RK2 and 2EPCO_6Y8Q has three hydrogen bond with the amino acid residue UNKO:H (2.3Å),UNKO:H(3.0Å) and UNKO:H(3.0Å) Meanwhile for the standard drug ligand-protein complexes cycloserine_6PXZ cycloserine_6RK2 and cycloserine_6Y8Q has five, six and one hydrogen bond. With the following amino acid; for cycloserine_6PXZ A:SER50(2.1Å), A:ASP51(2.2Å), A:SER50(2.3Å), UNKO:N(3.2Å), UNKO:N(3.2Å), UNKO:O(3.2Å), for cycloserine_6RK2 B:GLU367(3.2Å), B:ASN178(2.1Å), B:-GLU367(3.3Å), B:TYR307(3.3Å), B:ASN235(2.5Å), B:SER179(3.0Å), and for cycloserine_6Y8Q C:GLN88(2.2 Å), respectively. From the binding affinities presented in Table 7, it can be deduced that based on the highest affinities of 2EPCO over the commercial drug (CYCLO) it can be employ as a potential drug candidate for the treatment of bacterial infections.

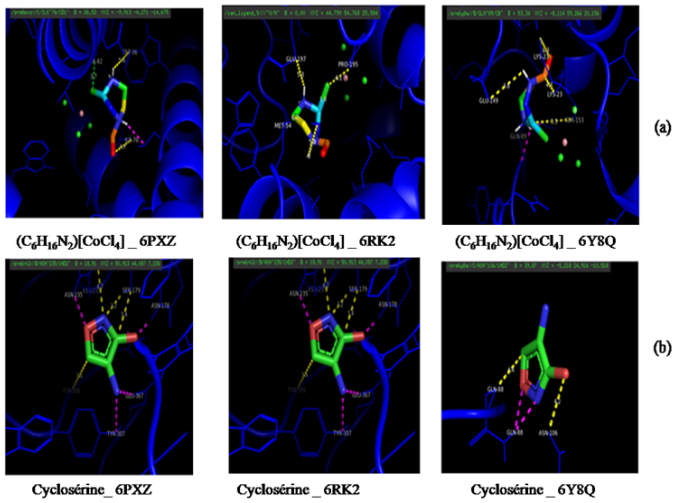

Figure S11: Pymol of the target receptors (6PXZ, 6RK2) with the title compound (a) and with the conventional Drug (Cycloserine) (b)

Conclusion

Finally, the present compound $(C_6H_{16}N_2)[CoCl_4]$ was prepared as single crystals at room temperature and characterized by physicochemical methods. On the structural level, the atomic arrangement of this material consists of a network of $[CoCl_4]^{2-}$ anions and 1-(2- ethylpiperazium) cations $[C_6H_{16}N_2]^{2+}$ connected by N–H···Cl and C –H···Cl hydrogen bonding interactions. The electronic properties, molecular docking, and Hirshfeld surface analysis of a single cobalt (Co) structure 2EPCO have been studied, the notable results from this study includes. The natural bond orbitals, shows that they exist a strong intermolecular interaction between the orbitals of the structure, with a second order perturbation energy value of 126.79 kcal.mol-1. The quantum theory of atom in molecule showed the existence of a greater binding strength between atoms of the structure and that the bond between cobalt and chlorine is a partially covalent bond. The Hirshfeld surface analysis for this study reveals that the contribution of the hydrogen to chlorine contact of the studied structure is 98.3% which makes up the percentage for the intermolecular interaction in the structure. Moreover, the RDG and AIM approach suggests a good stability of 2EPCO. In addition, MEPs mapping is determined to predict the nucleophilic and electrophilic reactions also the hydrogen bonding

interactions of the present molecule. From the binding affinities obtained from the molecular docking, it can be deduced that based on the highest affinities of present compound, over the commercial drug (CYCLO) it can be employ as a potential drug candidate for the treatment of bacterial infections. The optical properties of 2EPCO compound were investigated by UV– Vis absorption and photoluminescence measurements and revealed

that the complex exhibits a violet luminescence at an excitation at 280 nm. A thermal study by ATD/TG analysis which highlights the decomposition ranges and the stability of title compound.

Acknowledgments

We are grateful to the Tunisian Ministry of Higher Education Scientific Research for the provided financial support

Supplementary Data

CCDC 2069448 contains all data related to this crystal.

Conflict of interest

The authors don't have any conflict of interest.

Highlights

- A Novel Organic-Inorganic Hybrid Compound ($C_6H_{16}N_2$) [$CoCl_4$] was successfully synthesized and structurally characterized.
- The weak intermolecular interactions of (C6H16N2) [CoCl4] were studied by AIM, RDG, NBO and HS analysis.
- Optical properties UV-Visible and photoluminescence show that our synthesized compound is semiconductor (1.3 eV) and exhibits violet luminescence.
- The interaction between the ligand and the receptor proteins has the following binding affinities: 5 kcal.mol-1, -6 kcal.mol-1 and -5 kcal.mol-1 for 2EPCO_6PXZ, 2EPCO_6RK2, and 2EPCO_6Y8Q protein-complex interactions, respectively.

References

1. Lobo, V., Patil, A., Phatak, A., & Chandra, N. (2010). Free radicals, antioxidants and functional foods: Impact on human health. Pharmacognosy Reviews, 4, 118.
2. Azam, M., Al-Resayes, S. I., Wabaidur, S. M., Altaf, M., Chaurasia, B., et al. (2018). Synthesis, structural characterization and antimicrobial activity of Cu (II) and Fe (III) complexes incorporating azo-azomethine ligand. Molecules, 23, 813.
3. Tsiepe, T. J., Kabanda, M. M., & Serobatse, K. (2015). Antioxidant properties of kanakugiol revealed through the hydrogen atom transfer, electron transfer and M^{2+} coordination ability mechanisms: A DFT study in vacuo and in solution. Food Biophysics, 10, 342–359.
4. Świderski, G., Jabłońska-Trypuć, A., Kalinowska, M., Świsłocka, R., Karpowicz, D., et al. (2020). Spectroscopic, theoretical and antioxidant study of 3d-transition metals (Co (II), Ni (II), Cu(II), Zn(II)) complexes with cichoric acid. Materials, 13, 3102.
5. Alzahrani, R., Althagafi, I., Alsoliemy, A., Abou-Melha, K. S., Alrefaei, A. F., Mersal, G. A., & El-Metwaly, N. (2021). Synthesis and characterization for new Mn (II) complexes; conductometry, DFT, antioxidant activity via enhancing superoxide dismutase enzymes that confirmed by in-silico and in-vitro ways. Journal of Molecular Structure, 1243, 130855.
6. Oueslati, Y., El Bakri, Y., Valkonen, A., García, C. J. G., & Smirani, W. (2021). Growth, single crystal investigation, Hirshfeld surface analysis, DFT studies, molecular docking, physico-chemical characterization and in vitro antioxidant activity of a novel hybrid complex. Journal of Solid-State Chemistry, 301, 122319.
7. Sheldrick, G. M. (2015). Acta Crystallographica Section A, 71, 3–8.
8. Sheldrick, G. M. (2015). Acta Crystallographica Section C, 71, 3–8.
9. Brandenburg, K. (1998). Diamond (Version 2.0) [Software]. Impact GbR, Bonn, Germany.
10. Chen, W., Sun, S., Liang, Y., & Song, J. (2009). Antioxidant property of quercetin–Cr (III) complex: The role of Cr (III) ion. Journal of Molecular Structure, 918(1–3), 194–197.
11. Lee, C., Yang, W., & Parr, R. G. (1988). Development of the Colle–Salvetti correlation-energy formula into a functional of the electron density. Physical Review B, 37(2), 785.
12. Dennington, R. D. II, Keith, T. A., & Millam, J. M. (2016). GaussView (Version 6.0.16) [Software]. Semichem Inc., Shawnee Mission, KS.
13. Lu, T., & Chen, F. (2012). Multiwfn: A multifunctional wavefunction analyzer. Journal of Computational Chemistry, 33(5), 580–592.
14. Wolff, S. K., Grimwood, D. J., McKinnon, J. J., Jayatilaka, D., & Spackman, M. A. (2007). CrystalExplorer (Version 2.1) [Software]. University of Western Australia, Perth.
15. 15. Hu, Z., Bang, Y. J., Ruhn, K. A., & Hooper, L. V. (2019). Molecular basis for retinol binding by serum amyloid A during infection. Proceedings of the National Academy of Sciences, 116, 19077–19082.
16. Wang, C., Ye, F., Chang, C., Liu, X., Wang, J., et al. (2019). Agrobacteria reprogram virulence gene expression by controlled release of host-conjugated signals. Proceedings of the National Academy of Sciences, 116(44), 22331–22340.
17. Beck, I. N., Usher, B., Hampton, H. G., Fineran, P. C., & Blower, T. R. (2020). Antitoxin autoregulation of M. tuberculosis toxin-antitoxin expression through negative cooperativity arising from multiple inverted repeat sequences. Biochemical Journal, 477(12), 2401–2419.
18. Dhieb, A. C., Janzen, D. E., Rzaigui, M., & Smirani Sta, W. (2014). 1-Phenylpiperazine-1,4-diium tetrachloridocobalt(II). Acta Crystallographica Section E: Crystallographic Communications, 70, m139.
19. Tahenti, M., Issaoui, N., Roisnel, T., Marouani, H., AlDossary, O., & Kazachenko, A. S. (2022). Self-assembly of a new cobalt complex, $(C_6H_{14}N_2)_3[CoCl_4]$ Cl: Synthesis, empirical and DFT calculations. Journal of King Saud University – Science, 34, 101807.
20. Baur, W. (1974). Acta Crystallographica Section B: Structural Crystallography and Crystal Chemistry, 30, 1191–1195.
21. Khanum, G., Fatima, A., Siddiqui, N., Agarwal, D. D., Butcher, R. J., et al. (2022). Single crystal, characterization and computational study of 2-amino-N-cyclopropyl-5-ethyl-thiophene-3-carboxamide. Journal of Molecular Structure, 1250, 131890.
22. Blanco, M. A., Martín Pendás, A., & Francisco, E. (2005). Interacting quantum atoms: A correlated energy decomposition scheme based on the quantum theory of atoms in molecules. Journal of Chemical Theory and Computation, 1(6), 1096–1109.
23. Juhás, M., & Zitko, J. (2020). Molecular interactions of pyrazine-based compounds to proteins. Journal of Medicinal Chemistry, 63(17), 8901–8916.
24. Yunta, M. J. (2017). It is important to compute intramolecular hydrogen bonding in drug design. American Journal of Modeling and Optimization, 5(1), 24–57.
25. 25. Klein, A., Garci, F., Chebbi, H., Rouzbeh, N., Rochels, L., Disch, S., et al. (2022). Structure, optical and magnetic

properties of the pyridinium cobaltate $(C_6H_9N_2)_2[CoCl_4]$. Inorganica Chimica Acta, 539, 111095.
26. Drissi, N., Dakhlaoui, I., Karoui, K., Zaghrioui, M., & Jomni, F. (2022). Vibrational spectroscopy, electrical, and thermal properties of $[N(CH_3)_4][N(C_2H_5)_4]CoCl_4$ compound. Applied Organometallic Chemistry, 36, e6621.
27. Dang, Y., Yang, L., Youxuan, S., Dongsheng, Y., Xiaolong, L., et al. (2015). Bulk crystal growth of hybrid perovskite material $CH_3NH_3PbI_3$. CrystEngComm, 17, 665–670.
28. Ben Moussa, O., Chebbi, H., & Zid, M. F. (2019). Synthesis, crystal structure, vibrational study, optical properties and Hirshfeld surface analysis of bis(2,6-diaminopyridinium) tetrachloridocobaltate(II) monohydrate. Journal of Molecular Structure, 1180, 72–80.
29. Silvarajoo, S., Osman, U. M., Kamarudin, K. H., Razali, M. H., Yusoff, H. M., et al. (2020). Dataset of theoretical molecular electrostatic potential (MEP), HOMO–LUMO band gap and experimental Cole–Cole plot of 4-(ortho-, meta- and para-fluorophenyl) thiosemicarbazide isomers. Data in Brief, 32, 106299.
30. Louis, H., Amodu, I. O., Unimuke, T. O., Gber, T. E., Isang, B. B., et al. (2022). Modeling of $Ca_{12}O_{12}$, $Mg_{12}O_{12}$, and $Al_{12}N_{12}$ nanostructured materials as sensors for phosgene (Cl_2CO). Materials Today Communications, 33, 103946.
31. Demircioğlu, Z., Kaştaş, Ç. A., & Büyükgüngör, O. (2015). Theoretical analysis (NBO, NPA, Mulliken population method) and molecular orbital studies (hardness, chemical potential, electrophilicity and Fukui function analysis) of (E)-2-((4-hydroxy-2-methylphenylimino) methyl)-3-methoxyphenol. Journal of Molecular Structure, 109, 1183–1195.
32. Osigbemhe, I. G., Oyoita, E. E., Louis, H., Khan, E. M., Etim, E. E., et al. (2022). Antibacterial potential of N-(2-furylmethylidene)-1,3,4-thiadiazole-2-amine: Experimental and theoretical investigations. Journal of the Indian Chemical Society, 99(9), 100597.
33. Khan, M. U., Ibrahim, M., Khalid, M., Qureshi, M. S., Gulzar, T., et al. (2019). First theoretical probe for efficient enhancement of nonlinear optical properties of quinacridone-based compounds through various modifications. Chemical Physics Letters, 715, 222–230.
34. Campbell, P. G., Abbey, E. R., Neiner, D., Grant, D. J., Dixon, D. A., et al. (2010). Resonance stabilization energy of 1,2-azaborines: A quantitative experimental study by reaction calorimetry. Journal of the American Chemical Society, 132(51), 18048–18050.
35. Autumn, K., et al. (2002). [Title unclear—please clarify]. Proceedings of the National Academy of Sciences, 99(117), 12252.
36. Baldwin, L., et al. (2007). [Title unclear—please clarify]. Journal of Molecular Biology, 371, 283.
37. Dillon, A. C., et al. (1997). [Title unclear—please clarify]. Nature, 386, 377.
38. Johnson, E. R., Keinan, S., Mori-Sánchez, P., Contreras-García, J., Cohen, A. J., et al. (2010). [Title unclear—please clarify]. Journal of the American Chemical Society, 132, 6498–6506.
39. Contreras-García, J., Yang, W., & Johnson, E. R. (2011). Analysis of hydrogen-bond interaction potentials from the electron density: Integration of noncovalent interaction regions. Journal of Physical Chemistry A, 115, 12983–12990.
40. Humphrey, W., Dalke, A., & Schulten, K. (1996). VMD: Visual molecular dynamics. Journal of Molecular Graphics, 14, 33–38.
41. Lu, T., & Chen, F. (2012). Multiwfn: A multifunctional wavefunction analyzer. Journal of Computational Chemistry, 33, 580–592.
42. Huang, M., Li, C., & Evangelista, F. A. (2021). Theoretical calculation of core-excited states along dissociative pathways beyond second-order perturbation theory. Journal of Chemical Theory and Computation, 18(1), 219–233.
43. Kirfel, A., Lippmann, T., Blaha, P., Schwarz, K., Cox, D. F., et al. (2005). Electron density distribution and bond critical point properties for forsterite, Mg_2SiO_4, determined with synchrotron single-crystal X-ray diffraction data. Physics and Chemistry of Minerals, 32(4), 301–313.
44. Akman, F., Issaoui, N., & Kazachenko, A. S. (2020). Intermolecular hydrogen bond interactions in the thiourea/water complexes (Thio-(H_2O)) (n = 1, 5): X-ray, DFT, NBO, AIM, and RDG analyses. Journal of Molecular Modeling, 26(6), 116.
45. Bianchi, R., Gervasio, G., & Marabello, D. (2000). Experimental electron density analysis of $Mn_2(CO)_{10}$: Metal–metal and metal–ligand bond characterization. Inorganic Chemistry, 39(11), 2360–2366.
46. Tsushima, S. (2011). On the "yl" bond weakening in uranyl (VI) coordination complexes. Dalton Transactions, 40(25), 6732–6737.
47. Ejuh, G. W., Tchangnwa Nya, F., Djongyang, N., & Ndjaka, J. M. B. (2018). Study of some properties of quinone derivatives from quantum chemical calculations. Optical and Quantum Electronics, 50(9), 1–19.